Estimation of Serotonin Transporter Parameters with ^{11}C-DASB in Healthy Humans: Reproducibility and Comparison of Methods

W. Gordon Frankle[1], Mark Slifstein[1], Roger N. Gunn[2], Yiyun Huang[1,3], Dah-Ren Hwang[1,3], E. Ashlie Darr[1], Rajesh Narendran[1], Anissa Abi-Dargham[1,3], and Marc Laruelle[1,3]

[1]*Department of Psychiatry, Columbia University College of Physicians and Surgeons and the New York State Psychiatric Institute, New York, New York;* [2]*Translational Medicine and Genetics, GlaxoSmithKline, Greenford, United Kingdom; and* [3]*Department of Radiology, Columbia University College of Physicians and Surgeons and the New York State Psychiatric Institute, New York, New York*

The aim of the present study was to define the optimal analytic method to derive accurate and reliable serotonin transporter (SERT) receptor parameters with ^{11}C-3-amino-4-(2-[(dimethylamino)methyl]phenylthio)benzonitrile (^{11}C-DASB). **Methods:** Nine healthy subjects (5 females, 4 males) underwent two ^{11}C-DASB PET scans on the same day. Five analytic methods were used to estimate binding parameters in 10 brain regions: compartment modeling with 1- and 2-tissue compartment models (1TC and 2TC), data-driven estimation of parametric images based on compartmental theory (DEPICT) analysis, graphical analysis, and the simplified reference tissue model (SRTM). Two variations in the fitting procedure of the SRTM method were evaluated: nonlinear optimization and basis function approach. The test/retest variability (VAR) and intraclass correlation coefficient (ICC or reliability) were assessed for 3 outcome measures: distribution volume (V_T), binding potential (BP), and specific to nonspecific equilibrium partition coefficient (V_3''). **Results:** All methods gave similar values across all regions. The variability of V_T was excellent ($\leq$10%) in all regions, for the 1TC, 2TC, DEPICT, and graphical approaches. The variability of BP and V_3'' was good in regions of high SERT density and poorer in regions of moderate and lower densities. The ICC of all 3 outcome measures was excellent in all regions. The basis function implementation of SRTM demonstrated improved reliability compared with nonlinear optimization, particularly in moderate and low-binding regions. **Conclusion:** The results of this study indicate that ^{11}C-DASB can be used to measure SERT parameters with high reliability and low variability in receptor-rich regions of the brain, with somewhat less reliability and increased variability in regions of moderate SERT density and poor reproducibility in low-density regions.

Key Words: serotonin transporter; ^{11}C-DASB; PET; kinetic modeling; reproducibility

J Nucl Med 2006; 47:815–826

Recently, Wilson et al. (*1*) and Ginovart et al. (*2*) introduced ^{11}C-3-amino-4-(2-[(dimethylamino)methyl]phenylthio)benzonitrile (^{11}C-DASB), a new PET radiotracer to image the serotonin transporter (SERT). ^{11}C-DASB has emerged as the current PET radiotracer of choice to quantify SERT in clinical studies, such as methylenedioxymethamphetamine users (*3*), patients with depression (*4*), and patients with schizophrenia (*5*). Despite this the test/retest reproducibility of ^{11}C-DASB binding parameters estimates in the human brain have not been reported yet.

The aim of the present study was to evaluate the reproducibility of SERT receptor parameters' derivation with ^{11}C-DASB in regions of high, moderate, and low SERT density. Nine healthy volunteers were studied twice on the same day after injection of ^{11}C-DASB. Five approaches were compared for measurement of SERT receptor parameters: kinetic 1- and 2-tissue compartment (1TC and 2TC) models, a simplified reference tissue model (SRTM) (*6*), DEPICT (*7*), and graphical analysis (*8*). Three outcome measures were compared: total distribution volume (V_T), binding potential (BP), and specific-to-nonspecific equilibrium partition coefficient (V_3''). The comparison included the following attributes of the outcome measures: their identifiability, which describes the degree of certainty in parameter estimation, as well as the variability and reliability, which were assessed with test/retest reproducibility studies.

MATERIALS AND METHODS

Human Subjects

The study was approved by the Institutional Review Boards of the New York State Psychiatric Institute and Columbia Presbyterian Medical Center. Nine healthy volunteers participated in this study (age, 29 $\pm$ 8 y; range, 19–40 y, with these and subsequent values given as mean $\pm$ SD, 4 males, 5 females). All scans were performed between June 5, 2002, and March 10, 2003. All subjects recruited into the study are included in the analysis. The absence of pregnancy, medical, neurologic, and psychiatric history

(including alcohol and drug abuse) was assessed by history, review of systems, physical examination, routine blood tests including pregnancy test, urine toxicology, and electrocardiogram. Subjects provided written informed consent after receiving an explanation of the study.

Radiochemistry

The standard DASB and precursor desmethyl DASB were a gift from the University of Toronto. Preparation of ^{11}C-DASB followed the literature procedure, with some modifications (1,9).

The chemical purity of ^{11}C-DASB was 98.9% ± 1.1% and the radiochemical purity was 94.8% ± 2.5%.

PET Protocol

Each subject underwent 2 scans with ^{11}C-DASB on the same day. An arterial catheter was inserted into the radial artery after completion of the Allen test and infiltration of the skin with 1% lidocaine. A venous catheter was inserted in a forearm vein on the opposite side. Head movement minimization was achieved with a polyurethane head immobilization system (Soule Medical) (10). PET was performed with the ECAT EXACT HR+ (Siemens/CTI). A 10-min transmission scan was obtained before radiotracer injection. ^{11}C-DASB was injected intravenously over 45 s. Emission data were collected in 3-dimensional mode for 120 min as 21 successive frames of increasing duration (3×20 s, 3×1 min, 3×2 min, 2×5 min, 10×10 min). Subjects were allowed to rest outside of the camera for 30–45 min between the 2 injections.

Input Function Measurement

After radiotracer injection, arterial samples were collected every 10 s with an automated sampling system for the first 2 min and manually thereafter at longer intervals. A total of 32 samples were obtained per scan. After centrifugation (10 min at 1,800g), plasma was collected in 200-μL aliquots and activities were counted in a γ- counter (model 1480 Wizard 3M Automatic γ-Counter; Wallac).

Six samples (collected at 16, 30, 50, 70, 90, and 120 min) were further processed by high-pressure liquid chromatography to measure the fraction of plasma activity representing unmetabolized parent compound (9).

A biexponential function was fitted to the 6 measured unmetabolized fractions and used to generate a continuous measure of the parent fraction in plasma. The smallest exponential of the unmetabolized fraction curve, λ_{par}, was constrained to the difference between λ_{cer}, the terminal rate of washout of cerebellar activity, and λ_{tot}, the smallest elimination rate constant of the total plasma activity (11).

The input function, the initial distribution volume (V_{bol}, L), and the clearance of the parent compound (C_L, L/h) were calculated following published methodology (9,12).

The plasma free fraction (f_1) was determined as previously described (5,13).

MRI Acquisition and Segmentation Procedures

MR images were acquired and segmentation was performed following previously published methods (5,14).

Image Analysis

Images were reconstructed to a $128 \times 128 \times 63$ matrix (voxel size of $1.7 \times 1.7 \times 2.4$ mm) with attenuation correction using the transmission data and a Shepp 0.5 filter. Reconstructed image files were then processed with the image analysis software

MEDx (Sensor Systems, Inc.). All frames were realigned to a frame of reference, using a least-squares algorithm for within-modality coregistration (automated image registration [AIR]) (15). After frame-to-frame registration, the 21 frames were summed to generate a single data volume, which was coregistered to the MRI dataset using AIR (15). The spatial transformation derived from the summed PET registration procedure was then applied to each registered frame. Thus, each PET frame was resampled in the coronal plane to a voxel volume of $1.5 \times 0.9 \times 0.9$ mm^3.

Regions of interest (ROIs, $n = 10$) and region of reference (cerebellum) boundaries were drawn on the MR image according to criteria derived from brain atlases (16,17) and published reports (18–21). A segmentation-based method was used for the neocortical regions and a direct identification method was used for the subcortical regions (14).

The neocortical regions ($n = 6$) were as follows: dorsolateral prefrontal cortex (DLPFC, 30,753 ± 7,102 mm^3), medial prefrontal cortex (MPFC, 7,268 ± 3,275 mm^3), orbitofrontal cortex (OFC, 16,099 ± 3,535 mm^3), anterior cingulate cortex (ACC, 4,752 ± 2,223 mm^3), temporal cortex (TC, 54,225 ± 10,743 mm^3), and occipital cortex (OC, 43,804 ± 8,066 mm^3).

The subcortical regions ($n = 5$) included striatum (STR, 21,607 ± 3,340 mm^3), thalamus (THA, 9,925 ± 1,636 mm^3), midbrain (MID, 6,796 ± 623 mm^3), medial temporal lobe (MTL, 24,919 ± 2,923 mm^3; a spatially weighted average of 5 limbic structures, the uncus, amygdala, entorhinal cortex, parahippocampal gyrus, and hippocampus), and cerebellum (CER, 35,281 ± 12,200 mm^3). For bilateral regions, right and left values were averaged. The ROIs were a priori divided into 3 categories: regions with high SERT densities (MID, THA, STR), regions of moderate density (MTL and cingulate), and regions of low density (neocortical regions).

The contribution of total plasma activity to the regional time–activity data was calculated assuming a 5% blood volume in the ROIs (22), and tissue activities were calculated as the total regional activities minus the plasma contribution.

Derivation of Distribution Volumes

Kinetic Analysis. For the kinetic analysis, both a 2-compartment model (i.e., 1TC) and a 3-compartment model (i.e., 2TC) were used. The 2TC model included the arterial plasma compartment (C_a), the intracerebral free and nonspecifically bound compartment (nondisplaceable compartment (C_2), and the specifically bound compartment (C_3). The 1TC model included the arterial plasma compartment (C_a) and 1 tissue compartment (C_T), which includes C_2 and C_3. The total regional distribution volume (V_T, mL g^{-1}) was defined as the ratio of the tracer concentration in the region to the metabolite corrected plasma concentration at equilibrium:

$$V_T = \frac{C_T}{C_a}.$$

Data were fitted to the solutions of differential equations (23), and V_T was derived via a nonlinear regression using a Levenberg–Marquart least-squares minimization procedure (24), implemented in MATLAB (The Math Works, Inc.), and was used for the1TC model. For the 2TC, sequential quadratic programming with bound (nonnegativity) constraint, also implemented in MATLAB, was applied. The constraint was used because we found, as previously reported by others (2), that an unconstrained

2TC failed to reliably converge. For each of these, the squared residuals in the least-squares procedure were weighted in proportion to frame duration.

DEPICT Analysis. DEPICT (*7*) is a data driven method of parameter estimation that employs the basis pursuit concept (*25*). This method uses a basis function fitting procedure (*26,27*), in which an arbitrary number of basis functions can be used to fit the data due to an additional penalty term in the cost function that induces a sparse representation. DEPICT can be applied to plasma input or reference region input models, but only the plasma input models are presented here. The DEPICT V_T is derived simply from the integral of the estimated impulse response function. DEPICT was implemented with 30 kinetic basis functions whose exponential coefficients ranged from 0.6 to 0.014 min^{-1}. The relaxation parameter was fixed at a single value for all analyses based on an assessment of the leave-one-out cross-validation cost functions for all datasets. Again, data were weighted in proportion to frame duration.

Graphical Method. Graphical determination of V_T was performed by the method of Logan et al. (*8*). The determination of t*, the time from which the regression was computed, was performed by visual inspection.

Model Order and Goodness of Fit. For the 1TC and 2TC, goodness of fit of models with different levels of complexity were compared using the Akaike Information Criterion (AIC) (*28*) and the F test (*29,30*). DEPICT automatically determines model order as part of the fitting procedure based on the number of components that make a substantial contribution to the impulse response function.

Derivation of SERT Parameters

Derivation of SERT parameters was based on the following assumptions: (i) because of the negligible density of SERT in the cerebellum (*31–33*), cerebellum V_T was assumed to be representative of equilibrium nonspecific binding; (ii) the nonspecific binding did not vary significantly between regions.

The binding potential (BP) (*22*) was derived as the difference between V_T in the ROI ($V_{T\ ROI}$) and V_T in the cerebellum ($V_{T\ CER}$), the reference region. The relationship between BP and SERT receptor parameters is given by (*34*):

$$BP = \frac{f_1 B_{max}}{K_d},$$

where B_{max} is the regional concentration of SERT (nmol/L), and K_d is the in vivo affinity of the tracer for SERT (nmol/L).

For all plasma input methods, the specific-to-nonspecific equilibrium partition coefficient (V_3'') was derived as the ratio of BP to $V_{T\ CER}$. The relationship between V_3'' and SERT receptor parameters is given by (*34*):

$$V_3'' = \frac{f_2 B_{max}}{K_d},$$

where f_2 is the free fraction of the nonspecific distribution volume in the brain ($f_2 = f_1/V_{T\ CER}$).

V_3'' was also estimated by the simplified reference tissue method (SRTM) (*6*). SRTM uses assumptions (i) and (ii) to infer a functional relationship between a reference region (cerebellum) and an ROI. Because this method uses only brain data and not

plasma data, V_3'' is the only receptor-related parameter that can be estimated.

SRTM was applied without blood volume correction, the setting in which it would most typically be used. Two implementations of SRTM were tested. The first used an iterative optimization algorithm based on the Levenberg–Marquart procedure with fitting weights proportional to frame duration. The second implementation used a basis function approach implemented as described with 100 kinetic basis functions whose exponential coefficients ranged from 0.6 to 0.014 min^{-1} (*26*).

Evaluation of Methods

Results were evaluated according to 2 criteria: variability and reliability.

Variability. The test/retest variability (VAR) was calculated as the absolute value of the difference between the test and retest, divided by the mean of the test and retest values.

Reliability. To evaluate the within-subject variability relative to the between-subject variability, both within-subject SD (WSSD) and between-subject SD (BSSD) were calculated and expressed as percentage of mean value (WS %CV and BS %CV, where CV is coefficient of variation). The reliability of the measurements was assessed by the intraclass correlation coefficient (ICC) calculated as (*35*):

$$\frac{BSMSS - WSMSS}{BSMSS + WSMSS},$$

where BSMSS is the mean sum of square between subjects and WSMSS is the mean sum of square within subjects. This statistic estimates the relative contributions of between- and within-subject variability and assumes values from −1 (i.e., BSMSS = 0) to 1 (identity between test and retest, i.e., WSMSS = 0).

In addition, the numeric identifiability of the total distribution volume was examined for the 1TC and 2TC models. V_T identifiability statistics were derived as the square root of the quadratic form $\nabla_k(V_T)' C \nabla_k(V_T)$, where $\nabla_k(V_T)$ is the gradient of the outcome measure V_T with respect to the rate constants and **C** is the covariance matrix (inverse of the Fisher information matrix) of the rate constants (*29,30*), expressed as % of the respective parameters (%CV).

Statistical Analysis

The average of the test and retest values was calculated for each subject (*n* = 9) and the results are given as mean ± SD of these 9 average measurements. This allows for estimation of the variability in the population (i.e., between-subject SD). When the SD refers to variability between experiments rather than between subjects, the SD is followed by *n* = 18. Dependent variables were analyzed using repeated-measures ANOVA (RM ANOVA). A 2-tailed probability value of 0.05 was selected as the significance level.

RESULTS

Injected Dose

The injected dose (529.1 ± 62.9 MBq, *n* = 18), injected mass (5.4 ± 2.2 μg, *n* = 18), and specific activity (35.37 ± 21.94 GBq/μmol, *n* = 18) did not differ between the test and retest conditions (RM ANOVA, *P* = 0.82, 0.22, and 0.10, respectively).

Plasma Analysis

After an initial, rapid distribution phase, total plasma activity stabilized at a relatively constant level (Fig. 1A). ^{11}C-DASB underwent significant metabolism over the duration of the study (Fig. 1B). At 30 min, $34\% \pm 8\%$ of the total activity corresponded to the parent compound. The initial distribution volume (V_{bol}) of ^{11}C-DASB was 40 ± 10 L. The estimated parent plasma input function (mean across 9 subjects) is shown in Figure 1C. The average parent plasma clearance rate was 163 ± 37 L·h^{-1}; the clearance rate for the test condition was slightly lower than for the retest condition (146 ± 44 L·h^{-1} vs. 179 ± 36 L·h^{-1}, $P = 0.02$). The test/retest variability for the clearance was $26\% \pm 18\%$ with an ICC = 0.42. The free fraction of ^{11}C-DASB in the plasma was $9.4\% \pm 1.5\%$ and did not differ between conditions ($n = 18$, $P = 0.89$); test/retest variability = $13\% \pm 14\%$, ICC = 0.40.

Brain Analysis

Activity peaked relatively early in the cerebellum and neocortical regions (~25 min) and later in the STR, MID, and THA (35–55 min) with intermediate values in the limbic regions (25–35 min). The degree of tracer washout, defined as the percentage decrease from the peak activity to the end of the scan, was high in most regions (37%–65%) with the exception of the SERT dense MID, where the washout was notably lower ($16\% \pm 7\%$). The average ratios of ROI to cerebellar activity from 75 to 115 min were MID, 3.06 ± 0.45; THA, 2.26 ± 0.23; STR, 2.18 ± 0.21; MTL, 1.67 ± 0.19; ACC, 1.36 ± 0.16; and 1.25 ± 0.13, 1.13 ± 0.11, 1.12 ± 0.11, 1.09 ± 0.16, 1.08 ± 0.11 in the TC, OC, MPFC, OFC, and DLPFC, respectively.

1TC and 2TC Kinetic Analysis

The results from 1TC and 2TC analyses are shown in Tables 1 and 2, respectively. The 1TC model reached convergence for every study in all regions ($n = 198$). As stated earlier, an unconstrained 2TC model resulted in a high degree of nonconvergence. Only 22 of 198 regions converged (11%), with poor identifiability in most regions where convergence was obtained (identifiability < 10% in only 5 regions). Using the constrained 2TC model, convergence was achieved in all regions ($n = 11$) in each study ($n = 18$).

Cerebellum Distribution Volume. Neither the 1TC nor the 2TC model demonstrated an advantage in goodness of fit for this region, as illustrated in Figure 2. The cerebellar V_T calculated by the 1TC and 2TC were nearly identical. The V_T identifiability was similar for both the 1TC ($1.58\% \pm 0.44\%$) and the 2TC ($2.37\% \pm 0.71\%$) models. The test/retest variability and reliability were also similar across methods, with VAR of <10% and ICC of >0.9 in all cases. Given the similarities between the 1TC and 2TC, neither model provided an improved cerebellar fit. Therefore, when determining the regional SERT receptor parameters by the 1TC or 2TC model, the same model used for the regional fit was used for the cerebellum fit.

ROI Distribution Volumes. As illustrated in Figure 2, the fits achieved in each ROI with either the 1TC or 2TC kinetic model were similar. Given this similarity, V_T derived by either 1TC or 2TC analysis was nearly identical and highly correlated ($r^2 = 0.99$, $P < 0.0001$, $n = 180$). The regional mean identifiability for V_T was $1.69\% \pm 0.60\%$ ($n = 180$; range, $1.39\% \pm 0.53\%$ in THA to $2.33\% \pm 1.10\%$ in MID) with the 1TC model and $2.27\% \pm 0.88\%$ ($n = 180$; range, $1.54\% \pm 0.57\%$ in THA to $2.88\% \pm 0.83\%$ in the OFC) with the 2TC model. The variability of V_T derived by either model was excellent. The average VAR in V_T derived with the 1TC was $7.5\% \pm 0.9\%$; for the 2TC, the average VAR in V_T was $7.4\% \pm 1.0\%$. The ICC values of V_T for the 1TC and 2TC were excellent and identical at 0.93 ± 0.02.

SERT Parameter Analysis. The 1TC and 2TC models provided similar estimates of BP as well as similar estimates of V_3'' (Tables 1 and 2).
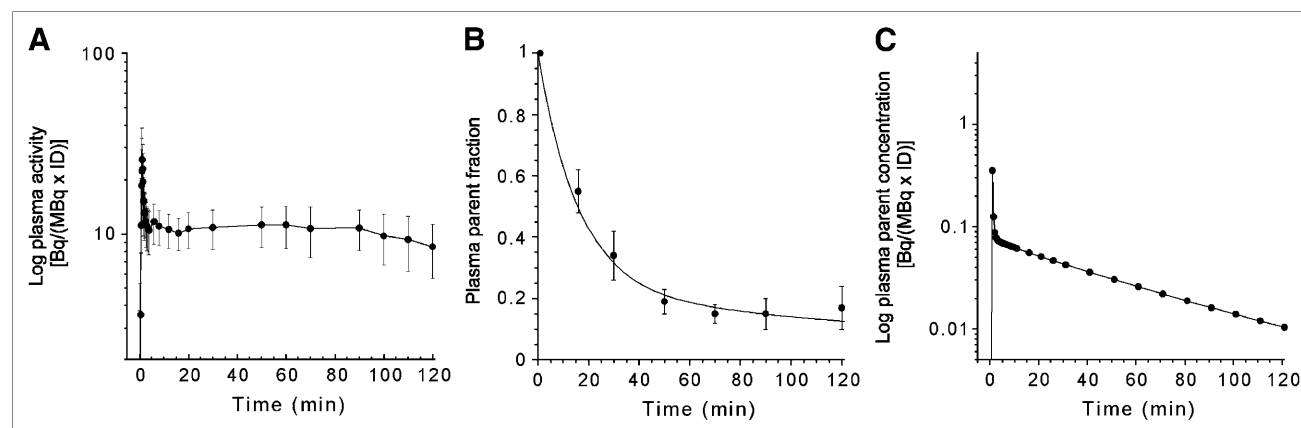
FIGURE 1. (A) Mean $\pm$ SD of total plasma activity normalized to injected dose [Bq/(mL $\times$ MBq ID) after injection of ^{11}C-DASB. Each point is mean of 9 subjects. After a rapid distribution, plasma activity stabilized to a relatively constant level. (B) Mean $\pm$ SD of fraction of plasma activity corresponding to parent compound after injection of ^{11}C-DASB. Values are mean of 9 subjects. (C) Mean plasma activity corresponding to parent compound after injection of ^{11}C-DASB. Each point is mean of 9 subjects.

TABLE 1
Reproducibility of ^{11}C-DASB Total Distribution Volume (V_T, mL·g^{-1}), Binding Potential (BP, mL·g^{-1}), and Specific-to-Nonspecific Equilibrium Partition Coefficient (V_3'', Unitless) Derived via 1TC Kinetic Model

SERT density region		V_T (mL·g^{-1})					BP (mL·g^{-1})					V_3'' (unitless)				
		Mean	BSSD (%CV)	WSSD (%CV)	VAR ± SD (%)	ICC	Mean	BSSD (%CV)	WSSD (%CV)	VAR ± SD (%)	ICC	Mean	BSSD (%CV)	WSSD (%CV)	VAR ± SD (%)	ICC
Reference	Cerebellum	9.6	2.00 (0.21)	0.39 (0.04)	7.6 ± 3.9	0.93	—	—	—	—	—	—	—	—	—	—
High (central)	Midbrain	29.9	7.59 (0.25)	1.02 (0.03)	5.9 ± 3.9	0.96	20.3	5.68 (0.28)	0.80 (0.04)	6.3 ± 4.2	0.96	2.09	0.22 (0.11)	0.08 (0.04)	6.5 ± 4.3	0.75
	Thalamus	19.7	4.26 (0.22)	0.86 (0.04)	8.1 ± 4.9	0.92	10.1	2.48 (0.25)	0.53 (0.05)	10.5 ± 5.0	0.91	1.05	0.13 (0.12)	0.04 (0.04)	5.7 ± 5.6	0.83
	Striatum	19.1	4.11 (0.21)	0.87 (0.05)	7.8 ± 5.2	0.91	9.5	2.31 (0.24)	0.52 (0.05)	8.8 ± 6.6	0.90	0.99	0.13 (0.13)	0.03 (0.03)	4.7 ± 3.3	0.91
Moderate (limbic)	Medial temporal lobe	14.4	3.46 (0.24)	0.51 (0.04)	6.1 ± 3.5	0.96	4.8	1.68 (0.35)	0.28 (0.06)	11.4 ± 7.1	0.95	0.49	0.11 (0.23)	0.04 (0.08)	12.5 ± 11.2	0.79
	Anterior cingulate	12.4	2.65 (0.21)	0.63 (0.05)	9.3 ± 4.9	0.89	2.7	0.89 (0.32)	0.31 (0.11)	21.5 ± 6.1	0.78	0.29	0.07 (0.26)	0.03 (0.09)	16.9 ± 9.6	0.79
Low (neocortex)	Temporal	11.2	2.32 (0.21)	0.43 (0.04)	7.3 ± 3.3	0.93	1.5	0.83 (0.54)	0.22 (0.14)	31.0 ± 31.9	0.87	0.16	0.09 (0.55)	0.02 (0.14)	31.7 ± 35.0	0.87
	DLPFC	10.4	2.03 (0.20)	0.40 (0.04)	7.4 ± 3.5	0.93	0.7	0.78 (1.07)	0.14 (0.20)	35.1 ± 36.2	0.93	0.08	0.08 (1.01)	0.01 (0.15)	33.4 ± 36.8	0.96
	MPFC	10.7	2.40 (0.22)	0.47 (0.04)	8.3 ± 4.5	0.93	1.1	0.75 (0.71)	0.15 (0.14)	53.2 ± 71.7	0.93	0.11	0.07 (0.65)	0.01 (0.12)	50.1 ± 73.4	0.94
	OFC	10.1	1.94 (0.19)	0.39 (0.04)	7.5 ± 2.3	0.92	0.5	0.95 (2.12)	0.22 (0.50)	54.0 ± 38.0	0.90	0.06	0.11 (2.01)	0.02 (0.38)	53.9 ± 37.3	0.93
	Occipital	10.6	2.25 (0.21)	0.42 (0.04)	7.5 ± 3.7	0.93	1.0	0.83 (0.88)	0.11 (0.12)	20.0 ± 19.0	0.97	0.10	0.09 (0.85)	0.01 (0.12)	22.1 ± 14.5	0.96

Values are mean of 9 subjects with each value measured twice.

The reproducibility for the outcome measures BP and V_3'' varied with regional SERT density. Tables 1 and 2 list the VAR and ICC for BP and V_3'' across regions of high, moderate, and low SERT density for each method. For both BP and V_3'', the test/retest variability increased as the SERT density of the region decreased. Overall, no difference in test/retest variability was observed between the methods for BP (RM ANOVA, $P = 0.30$) or V_3'' (RM ANOVA, $P = 0.22$). Unlike the variability, the reliability did not vary by regional SERT density. The reliability of BP (1TC, 0.91 ± 0.06; 2TC, 0.91 ± 0.05) and V_3'' (1TC, 0.87 ± 0.08; 2TC, 0.87 ± 0.09) was excellent across all regions.

Model Order Estimation. The models were compared for goodness of fit by the F test (*29,30*) and AIC (*28*). The F test was significant ($P < 0.05$) in 51 of the 198 (9 subjects × 2 studies × 11 regions) fits examined, indicating that the higher-order model (2TC) provided a better fit for 26% of the datasets. The F test was generally significant on a study basis rather than a regional basis. In other terms, in 4 of the 18 studies, the 2TC provided a better fit than the 1TC in most regions, whereas, in the other studies, no benefit of the higher-order model was observed in the majority regions. The AIC of the 2TC model was lower than the AIC of the 1TC in 115 of the 198 fits examine (58%), indicating a better fit. The AIC and the F test shared the property that, across all regions, some studies were fitted better with a 2TC model than with the 1TC model. In all cases, when the F test indicated a better fit using the higher-order model (51/198), this was confirmed by the AIC.

DEPICT Analysis

The results from the DEPICT analysis are shown in Table 3.

Cerebellum Distribution Volume. The DEPICT produced cerebellar V_T nearly identical to the 1TC and 2TC estimates (RM ANOVA, $P = 0.39$). Similarly, the variability was excellent with a VAR of <10% and ICC of >0.9 in each case.

ROI Distribution Volumes. Distribution volumes derived by DEPICT were highly correlated with the kinetic analysis (DEPICT = 1.00 × 2TC, $r^2 = 0.96$, $P < 0.0001$). Significant differences were observed between DEPICT and both the 1TC and 2TC models (RM ANOVA, $P < 0.0001$). Post hoc analysis revealed that the V_T derived with DEPICT was slightly, but significantly, lower than the 1TC or 2TC models only in the MID (e.g., 29.4 ± 7.2 mL·g^{-1} vs. 25.8 ± 4.8 mL·g^{-1}, 2TC MID vs. DEPICT MID; Fisher's protected least-significant difference [PLSD] post hoc test, $P = 0.0006$). No differences were observed between DEPICT and the kinetic models in any other region.

The reproducibility of V_T derived by DEPICT was similar to the 1TC and 2TC models, with a VAR of 7.8% ± 1.2% and ICC of 0.91 ± 0.02.

SERT Parameter Analysis. The SERT parameters derived by DEPICT were highly correlated with the kinetic analysis (BP, DEPICT = 1.02 × 2TC, $r^2 = 0.95$, $P < 0.0001$; V_3'',

TABLE 2
Reproducibility of ^{11}C-DASB Total Distribution Volume (V_T, mL·g^{-1}), Binding Potential (BP, mL·g^{-1}), and Specific-to-Nonspecific Equilibrium Partition Coefficient (V_3'', Unitless) Derived via 2TC Kinetic Model

SERT density region		Mean	BSSD (%CV)	WSSD (%CV)	VAR ± SD (%)	ICC	Mean	BSSD (%CV)	WSSD (%CV)	VAR ± SD (%)	ICC	Mean	BSSD (%CV)	WSSD (%CV)	VAR ± SD (%)	ICC
		V_T (mL·g^{-1})					BP (mL·g^{-1})					V_3'' (unitless)				
Reference	Cerebellum	9.5	2.00 (0.21)	0.39 (0.04)	7.7 ± 4.1	0.92	—	—	—	—	—	—	—	—	—	—
High (central)	Midbrain	29.4	7.32 (0.25)	1.01 (0.03)	5.9 ± 3.9	0.96	19.9	5.41 (0.27)	0.77 (0.04)	6.2 ± 4.4	0.96	2.07	0.22 (0.10)	0.09 (0.04)	6.5 ± 4.5	0.73
	Thalamus	19.5	4.21 (0.22)	0.85 (0.04)	8.1 ± 4.8	0.92	10.0	2.44 (0.24)	0.52 (0.05)	10.4 ± 4.7	0.91	1.05	0.13 (0.12)	0.04 (0.04)	5.3 ± 5.8	0.84
	Striatum	19.0	4.05 (0.21)	0.86 (0.05)	7.7 ± 5.2	0.91	9.4	2.26 (0.24)	0.51 (0.05)	8.6 ± 6.5	0.90	0.99	0.13 (0.13)	0.03 (0.03)	4.3 ± 3.6	0.92
Moderate (limbic)	Medial temporal lobe	14.2	3.40 (0.24)	0.50 (0.04)	5.9 ± 3.8	0.96	4.7	1.63 (0.35)	0.29 (0.06)	12.1 ± 8.6	0.94	0.49	0.11 (0.22)	0.04 (0.09)	13.3 ± 13.0	0.73
	Anterior cingulate	12.3	2.63 (0.21)	0.61 (0.05)	9.1 ± 4.7	0.90	2.7	0.87 (0.32)	0.30 (0.11)	20.3 ± 5.2	0.79	0.29	0.07 (0.26)	0.02 (0.08)	15.5 ± 10.2	0.81
Low (neocortex)	Temporal	11.1	2.30 (0.21)	0.42 (0.04)	7.1 ± 3.3	0.94	1.5	0.82 (0.54)	0.22 (0.14)	31.3 ± 30.9	0.87	0.16	0.09 (0.55)	0.02 (0.15)	32.1 ± 34.4	0.86
	DLPFC	10.3	2.03 (0.20)	0.39 (0.04)	7.3 ± 3.6	0.93	0.7	0.77 (1.07)	0.14 (0.19)	35.4 ± 44.8	0.94	0.08	0.08 (1.01)	0.01 (0.15)	35.1 ± 43.9	0.96
	MPFC	10.6	2.39 (0.23)	0.46 (0.04)	8.3 ± 4.6	0.93	1.0	0.74 (0.71)	0.14 (0.13)	57.1 ± 84.3	0.93	0.11	0.07 (0.65)	0.01 (0.12)	55.1 ± 87.3	0.94
	OFC	10.0	1.92 (0.19)	0.37 (0.04)	7.2 ± 2.2	0.93	0.5	0.96 (2.13)	0.22 (0.50)	54.8 ± 35.6	0.90	0.06	0.11 (2.02)	0.02 (0.42)	54.9 ± 36.0	0.92
	Occipital	10.5	2.24 (0.21)	0.41 (0.04)	7.5 ± 3.7	0.93	0.9	0.83 (0.88)	0.11 (0.12)	20.4 ± 18.7	0.97	0.10	0.09 (0.86)	0.01 (0.12)	22.7 ± 13.8	0.96

Values are mean of 9 subjects with each value measured twice.
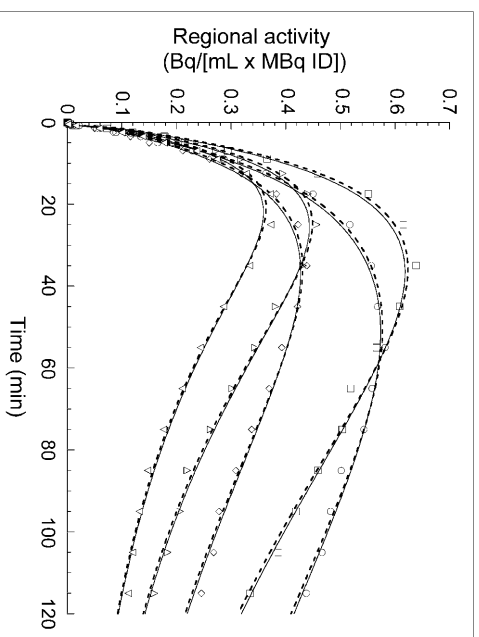
FIGURE 2. Regional time-activity curves measured after injection of 551.3 MBq ^{11}C-DASB in 33-y-old female. Regions displayed include MID (○), STR (□), MTL (◇), and CER (▽). Points are measured activities in ROIs; lines are fitted values to 1TC model (solid line) and 2TC model (dashed line). Fits for both models are similar.

DEPICT = 1.03 × 2TC, r^2 = 0.95, $P < 0.0001$). As with the V_T, both BP and V_3'' derived with DEPICT were significantly different than BP and V_3'' derived with the 1TC and 2TC (RM ANOVA $P < 0.0001$ for both BP and V_3''). Post hoc analysis revealed that BP and V_3'' derived with DEPICT were slightly, but significantly, lower than that derived with the kinetic models only in the MID (e.g., BP, 19.9 ± 5.4 mL·g^{-1} vs. 16.3 ± 3.2 mL·g^{-1}, 2TC MID vs. DEPICT MID; Fisher's PLSD, $P = 0.0005$). No differences were observed between DEPICT and the kinetic models in any other region. As with the kinetic models, the VAR for the outcome measures BP and V_3'' derived via DEPICT increased as the SERT density of the region decreased. Overall, no difference in VAR was observed between DEPICT and the kinetic methods for BP (RM ANOVA, $P = 0.43$) or V_3'' (RM ANOVA, $P = 0.43$). The ICC of BP (0.86 ± 0.05) and V_3'' (0.82 ± 0.09), though still excellent, were slightly, but significantly, lower than those of the kinetic models (RM ANOVA, $P < 0.0001$ and $P = 0.03$, respectively).

Model Order Estimation. The DEPICT plasma input method selected a 1TC model in 70 of the 198 fits, a 2TC model in 125 of the 198 fits, and a 3-tissue compartment (3TC) model in 3 of the 198 fits.

Graphical Analysis

The results from the graphical analysis are shown in Table 4.

Cerebellum Distribution Volume. The graphical analyses also produced cerebellar V_T similar to the 1TC and 2TC estimates. The reproducibility of the cerebellar distribution volume derived with the graphical analysis was excellent, with a VAR of <10% and an ICC of >0.9 in each case.

TABLE 3
Reproducibility of ^{11}C-DASB Total Distribution Volume (V_T, mL·g^{-1}), Binding Potential (BP, mL·g^{-1}), and Specific-to-Nonspecific Equilibrium Partition Coefficient (V_3'', Unitless) Derived via DEPICT Analysis

SERT density region		V_T (mL·g^{-1})					BP (mL·g^{-1})					V_3'' (unitless)				
		Mean	BSSD (%CV)	WSSD (%CV)	VAR ± SD (%)	ICC	Mean	BSSD (%CV)	WSSD (%CV)	VAR ± SD (%)	ICC	Mean	BSSD (%CV)	WSSD (%CV)	VAR ± SD (%)	ICC
Reference	Cerebellum	9.6	1.83 (0.19)	0.38 (0.04)	7.1 ± 3.2	0.92	—	—	—	—	—	—	—	—	—	—
High (central)	Midbrain	25.8	4.82 (0.19)	1.03 (0.04)	7.2 ± 3.0	0.91	16.3	3.22 (0.20)	0.75 (0.05)	8.5 ± 3.9	0.90	1.71	0.21 (0.12)	0.06 (0.04)	6.2 ± 5.0	0.83
	Thalamus	19.6	4.11 (0.21)	1.07 (0.05)	9.8 ± 5.6	0.87	10.0	2.53 (0.25)	0.83 (0.08)	14.6 ± 9.6	0.80	1.05	0.16 (0.15)	0.08 (0.07)	11.5 ± 9.6	0.64
	Striatum	18.9	3.75 (0.20)	0.98 (0.05)	9.5 ± 4.4	0.87	9.3	2.12 (0.23)	0.68 (0.07)	12.9 ± 7.3	0.82	0.97	0.13 (0.14)	0.05 (0.05)	9.1 ± 5.2	0.76
Moderate (limbic)	Medial temporal lobe	14.2	3.04 (0.21)	0.58 (0.04)	7.3 ± 4.1	0.93	4.7	1.43 (0.31)	0.31 (0.07)	13.0 ± 7.4	0.91	0.49	0.10 (0.21)	0.03 (0.07)	12.4 ± 6.1	0.80
	Anterior cingulate	12.2	2.51 (0.21)	0.58 (0.05)	9.2 ± 4.0	0.90	2.6	0.88 (0.33)	0.30 (0.11)	21.5 ± 15.5	0.79	0.27	0.07 (0.27)	0.03 (0.11)	19.1 ± 14.5	0.71
Low (neocortex)	Temporal	11.2	2.10 (0.19)	0.46 (0.04)	7.3 ± 4.4	0.91	1.6	0.71 (0.45)	0.22 (0.14)	22.1 ± 11.9	0.82	0.17	0.08 (0.47)	0.02 (0.14)	20.9 ± 14.2	0.83
	DLPFC	10.4	2.01 (0.19)	0.41 (0.04)	7.1 ± 4.5	0.92	0.8	0.78 (0.93)	0.23 (0.27)	151.0 ± 196.2	0.84	0.09	0.08 (0.89)	0.02 (0.23)	153.7 ± 208.1	0.87
	MPFC	10.6	2.21 (0.21)	0.42 (0.04)	6.7 ± 5.1	0.93	1.1	0.72 (0.69)	0.15 (0.14)	39.4 ± 38.7	0.92	0.11	0.07 (0.64)	0.02 (0.14)	39.1 ± 34.2	0.91
	OFC	10.1	1.89 (0.19)	0.47 (0.05)	8.4 ± 3.8	0.88	0.6	1.02 (1.80)	0.28 (0.49)	45.9 ± 34.2	0.86	0.07	0.12 (1.76)	0.03 (0.41)	44.3 ± 39.0	0.90
	Occipital	10.5	2.09 (0.20)	0.44 (0.04)	6.8 ± 5.1	0.92	0.9	0.73 (0.78)	0.17 (0.18)	37.7 ± 34.9	0.89	0.10	0.08 (0.78)	0.02 (0.18)	41.5 ± 33.1	0.89

Values are mean of 9 subjects with each value measured twice.

ROI Distribution Volumes. The regional total distribution volumes derived with the graphical method were highly correlated with those derived via both 1TC and 2TC models ($r^2 = 0.99$, $P = 0.0001$, $n = 198$). Across regions, graphical V_T values were 100.4% ± 2.5% those of the 1TC model and 101.3% ± 2.5% those of the 2TC model. The variability and ICC for the graphical V_T data were similar to the kinetic models (variability, 8.3% ± 1.2%; ICC, 0.89 ± 0.03).

SERT Parameter Analysis. As with V_T, the regional values of BP and V_3'' derived by the graphical method were highly correlated with those derived by either 1TC or 2TC model (for both models, BP and V_3'': $r^2 = 0.99$, $P = 0.0001$, $n = 180$). A significant difference was observed for V_3'' derived via the 1TC and 2TC kinetic models compared with the graphical analysis (RM ANOVA, $P < 0.001$). Fisher PLSD post hoc analysis revealed significant differences ($P < 0.05$) in the high-binding regions (MID, THA, and STR), with the V_3'' values in these regions derived via the graphical analysis being 1.5%–2.7% lower than those derived via the 1TC or 2TC models. No difference in VAR was observed between the graphical and kinetic methods for BP (RM ANOVA, $P = 0.56$) or for V_3'' (RM ANOVA, $P = 0.55$). The ICC of BP (0.87 ± 0.08) and V_3'' (0.84 ± 0.08) was lower than observed with the kinetic models (RM ANOVA, $P = 0.0002$ and $P = 0.08$, respectively).

SRTM Analysis

The results from the SRTM analyses are shown in Table 5. V_3'' derived by the SRTM was highly correlated with plasma input based V_3'' (e.g., SRTM [iterative] vs. 2TC, $r^2 = 0.99$, $P < 0.0001$, $n = 180$). No difference in variability between the iterative method and the basis function method was seen (RM ANOVA, $P = 0.30$). The ICC observed with the iterative method was lower than that of the basis function method, although this did not reach the level of significance (iterative, 0.67 ± 0.26; basis, 0.81 ± 0.11, RM ANOVA, $P = 0.15$). A significant difference was observed in V_3'' values derived via the 1TC and 2TC kinetic models compared with SRTM (RM ANOVA, $P < 0.009$). Fisher PLSD post hoc analysis revealed significant differences ($P < 0.05$) in the high-binding regions (MID, THA, and STR), with the V_3'' values in these regions derived via SRTM being 5.8%–10.0% lower than those derived via the 1TC or 2TC model. Compared with the 1TC and 2TC models no difference was observed in the VAR measured for either SRTM method (RM ANOVA, $P = 0.08$). However, both SRTM analyses resulted in lower reliability than seen with the either the 1TC or 2TC models (RM ANOVA, $P < 0.0001$).

Across Method Comparison of V_3''

Table 6 provides the correlation between each of the 6 methods used to derived V_3'' in this study. The r^2 values listed in Table 6 are the square of the Pearson correlation coefficient determined between each method, for each subject, across all ROIs ($n = 180$). Excellent agreement

TABLE 4
Reproducibility of ^{11}C-DASB Total Distribution Volume (V_T, mL·g^{-1}), Binding Potential (BP, mL·g^{-1}), and Specific-to-Nonspecific Equilibrium Partition Coefficient (V_3'', Unitless) Derived via Graphical Analysis

	SERT density region	V_T (mL·g^{-1})					BP (mL·g^{-1})					V_3'' (unitless)				
		Mean	BSSD (%CV)	WSSD (%CV)	VAR ± SD (%)	ICC	Mean	BSSD (%CV)	WSSD (%CV)	VAR ± SD (%)	ICC	Mean	BSSD (%CV)	WSSD (%CV)	VAR ± SD (%)	ICC
Reference	Cerebellum	9.7	1.93 (0.20)	0.42 (0.04)	8.0 ± 3.2	0.91	—	—	—	—	—	—	—	—	—	—
High (central)	Midbrain	29.4	6.64 (0.23)	1.02 (0.03)	6.0 ± 2.7	0.95	19.7	4.81 (0.24)	0.73 (0.04)	5.7 ± 3.4	0.95	2.04	0.19 (0.09)	0.07 (0.03)	5.1 ± 4.9	0.77
	Thalamus	19.5	3.99 (0.20)	1.07 (0.05)	9.7 ± 6.0	0.87	9.9	2.39 (0.24)	0.72 (0.07)	14.1 ± 9.1	0.83	1.02	0.15 (0.15)	0.06 (0.06)	9.7 ± 8.2	0.76
	Striatum	19.0	3.78 (0.20)	1.02 (0.05)	9.2 ± 5.2	0.86	9.3	2.12 (0.23)	0.68 (0.07)	11.9 ± 7.8	0.81	0.97	0.14 (0.14)	0.05 (0.05)	7.6 ± 6.0	0.79
Moderate (limbic)	Medial temporal lobe	14.5	3.26 (0.22)	0.67 (0.05)	7.4 ± 4.0	0.92	4.8	1.59 (0.33)	0.41 (0.09)	13.3 ± 8.3	0.87	0.50	0.11 (0.22)	0.04 (0.09)	13.3 ± 11.0	0.75
	Anterior cingulate	12.4	2.52 (0.20)	0.72 (0.06)	10.2 ± 4.9	0.85	2.8	0.86 (0.31)	0.37 (0.13)	23.4 ± 10.7	0.69	0.29	0.08 (0.26)	0.03 (0.10)	18.9 ± 11.3	0.76
Low (neocortex)	Temporal	11.2	2.18 (0.20)	0.48 (0.04)	7.6 ± 3.7	0.91	1.5	0.80 (0.54)	0.22 (0.15)	27.2 ± 20.4	0.86	0.16	0.09 (0.55)	0.02 (0.14)	28.8 ± 24.2	0.89
	DLPFC	10.4	1.93 (0.18)	0.51 (0.05)	8.8 ± 4.1	0.87	0.8	0.88 (1.12)	0.17 (0.21)	31.1 ± 18.7	0.93	0.11	0.09 (1.03)	0.01 (0.16)	32.0 ± 23.1	0.95
	MPFC	10.8	2.27 (0.21)	0.55 (0.05)	8.9 ± 4.9	0.89	1.1	0.76 (0.70)	0.19 (0.17)	50.8 ± 57.1	0.89	0.11	0.07 (0.66)	0.02 (0.15)	48.7 ± 56.8	0.90
	OFC	10.1	1.84 (0.18)	0.44 (0.04)	7.4 ± 4.0	0.89	0.5	0.98 (2.04)	0.25 (0.51)	51.9 ± 32.2	0.88	0.06	0.11 (1.91)	0.02 (0.40)	50.3 ± 30.3	0.92
	Occipital	10.6	2.09 (0.20)	0.45 (0.04)	7.7 ± 3.4	0.91	1.0	0.82 (0.84)	0.14 (0.15)	47.5 ± 43.0	0.94	0.10	0.09 (0.83)	0.02 (0.15)	47.5 ± 38.8	0.94

Values are mean of 9 subjects with each value measured twice.

existed across all methods, with the highest correlation seen between the 1TC, 2TC, and graphical methods.

DISCUSSION

The goal of this study was to evaluate the ability to accurately estimate regional SERT binding parameters with ^{11}C-DASB PET by repeating each subject's PET scan on the same day and assessing reproducibility indices.

Outcome Measures and Models

Three outcome measures were examined in this study: the total distribution volume (V_T), the binding potential (BP), and the specific-to-nonspecific partition coefficient (V_3''). V_T includes free and nonspecific as well as specific binding of the radiotracer so that its use as a direct outcome measure to infer binding properties should be restricted to situations where separate measurement of nonspecific binding is not possible (i.e., when no appropriate region of reference exists) and nonspecific binding is negligible relative to the specific binding (which is not the case for ^{11}C-DASB). Its most frequent use is in situations such as the present study where a reference region does exist, so that BP and V_3'' can be inferred indirectly in terms of V_T from the ROI and the region of reference. BP does not include tissue nonspecific binding but is proportional to f_1, the plasma free fraction, so that similar f_1 values across populations is a prerequisite for comparisons using this parameter. V_3'' is independent of f_1 but is proportional to f_2, the tissue free fraction, so that similar values of f_2 across populations are necessary for making comparisons with this parameter.

A range of modeling techniques was used to estimate the outcome measures for this study. In this study the kinetic analysis was performed by 2 techniques (both using the arterial input function). The first technique assumed a specific compartment model, either 1TC or 2TC, to yield estimates of the rate constants governing transfer between the compartments, which were subsequently used to derive the outcome measures. The second, DEPICT, made no a priori assumption regarding the compartment model but, rather, derived the model order from the data (7). The second analytic method used to derive SERT binding parameters in this study was by use of reference region input with SRTM. SRTM is also a model-based method that uses a region of reference—in this case, the CER—as the input function for the model (6). This method restricts the outcome measure to V_3'', with the attendant caveats regarding nonspecific binding. The final analytic method used in this study was graphical analysis (36), another data-driven method, in which a nonlinear transformation of the data leads to a linear relationship between the transformed variables, allowing determination of V_T via linear regression.

In all, 14 outcome measures were evaluated: V_T by 1TC, 2TC, DEPICT, and graphical methods; BP by 1TC, 2TC, DEPICT, and graphical methods; and V_3'' by a 1TC, 2TC,

TABLE 5
Reproducibility of ¹¹C-DASB Specific-to-Nonspecific Equilibrium Partition Coefficient (V_3'', Unitless) Derived via SRTM Analysis

		Iterative method					Basis function method				
SERT density	region	Mean	BSSD (%CV)	WSSD (%CV)	VAR ± SD (%)	ICC	Mean	BSSD (%CV)	WSSD (%CV)	VAR ± SD (%)	ICC
High (central)	Midbrain	1.88	0.18 (0.10)	0.06 (0.03)	5.0 ± 4.0	0.82	1.76	0.14 (0.08)	0.05 (0.03)	4.1 ± 3.5	0.81
	Thalamus	0.99	0.15 (0.15)	0.07 (0.07)	10.5 ± 10.0	0.66	0.99	0.14 (0.14)	0.07 (0.07)	10.9 ± 9.6	0.61
	Striatum	0.91	0.14 (0.16)	0.04 (0.04)	6.8 ± 5.0	0.86	0.91	0.14 (0.15)	0.04 (0.04)	7.2 ± 4.6	0.84
Moderate (limbic)	Medial temporal lobe	0.48	0.10 (0.21)	0.04 (0.09)	13.9 ± 11.9	0.70	0.48	0.09 (0.19)	0.04 (0.08)	13.2 ± 12.2	0.68
	Anterior cingulate	0.33	0.07 (0.20)	0.08 (0.26)	32.9 ± 32.4	−0.22	0.30	0.07 (0.22)	0.03 (0.10)	16.9 ± 11.4	0.64
Low (neocortex)	Temporal	0.16	0.08 (0.51)	0.02 (0.13)	24.0 ± 15.4	0.87	0.16	0.08 (0.47)	0.02 (0.13)	19.6 ± 12.7	0.86
	DLPFC	0.14	0.15 (1.03)	0.10 (0.66)	75.1 ± 82.9	0.41	0.09	0.08 (0.85)	0.02 (0.20)	197.3 ± 417.1	0.89
	MPFC	0.13	0.11 (0.83)	0.05 (0.38)	73.1 ± 76.5	0.65	0.12	0.07 (0.58)	0.02 (0.16)	40.7 ± 39.4	0.86
	OFC	0.12	0.15 (1.22)	0.06 (0.46)	75.4 ± 84.9	0.75	0.07	0.10 (1.48)	0.03 (0.38)	119.4 ± 197.5	0.87
	Occipital	0.12	0.08 (0.69)	0.03 (0.28)	49.0 ± 26.4	0.73	0.11	0.08 (0.73)	0.02 (0.19)	81.1 ± 145.6	0.87

Values are mean of 9 subjects with each value measured twice.

TABLE 6
Correlation of ¹¹C-DASB V_3'' Derived with Various Analytic Methods

Method	1TC	2TC	DEPICT	Graphical	SRTM iterative	SRTM basis
1TC	1					
2TC	0.9996	1				
DEPICT	0.9522	0.9532	1			
Graphical	0.9966	0.9966	0.9615	1		
SRTM iterative	0.9766	0.9760	0.9562	0.9814	1	
SRTM basis	0.9767	0.9785	0.9865	0.9831	0.9735	1

Values of are square of the Pearson correlation coefficient (r^2) for V_3'' values in every region of each study ($n = 180$).

DEPICT, graphical, and SRTM, with the SRTM analyses performed by 2 approaches, iterative and basis function. Two criteria were assessed, the reliability and variability. Variability is the between-scan differences observed within subjects and reliability relates to the relative contributions of within- and between-subject variability—that is, the ability to detect true between-subject differences given the level of within-subject variability.

Comparison of DEPICT with Kinetic Methods

One goal of this study was to compare the results produced by DEPICT with those obtained with the 1TC and 2TC models. Using either a 1TC or 2TC model to derive V_T, BP or V_3'' gave nearly identical results for each outcome measure across all regions. The regional values of the outcome measures derived by the DEPICT method were similar to both the 1TC and 2TC models but slightly lower in the MID region. The MID is the region with the highest SERT density and, therefore, the highest V_T. The DEPICT analysis resulted in a V_T of 25.8 ± 4.8 mL·g^{-1} in this region compared with 29.9 ± 7.6 mL·g^{-1} and 29.4 ± 7.3 mL·g^{-1} for the 1TC and 2TC models, respectively, with commensurately lower values of BP and V_3'' in the MID, but nearly identical values for these outcome measures in other regions. The reason for this is that DEPICT is a basis function method and includes, as do most basis function implementations, truncation of the set of exponential rate constants associated with the basis function set at a finite positive number slightly larger than the theoretic lower limit (i.e., zero for decay-corrected data or the decay constant for uncorrected data). This is because, in the presence of statistical noise, identifiability of distribution volume estimates becomes poor near this limit. However, the approach may be associated with a small amount of bias at the highest distribution volumes. The tradeoff is a great increase in the stability of the estimates. This becomes particularly apparent in voxelwise analysis, as opposed to ROI analysis, where basis function methods perform well, but the decreased signal-to-noise level becomes prohibitively

problematic for iterative methods. Also, given that both approaches used the same arterial input function data, the iterative methods do not necessarily represent a gold standard in this comparison. This issue needs to be further explored both through analysis of other datasets and by simulations in which "true" parameter values are known.

The VAR, of V_T was excellent (<10%) in all regions, for both kinetic approaches and DEPICT. Similarly, in regions of high SERT density, the variability of BP and V_3'' was also good (<10%). However, in regions of moderate and low SERT density, the variability associated with BP and V_3'' was higher than that of V_T. This is not unexpected, as BP and V_3'' are derived via the difference in V_T between the ROI and the region of reference, thereby increasing the effects of noise on the variability measurement. This is particularly evident when the V_T in the ROI is close to V_2, such as in the neocortical regions. In this study the variability of BP and V_3'' derived by the kinetic methods ranged from 14.4% ± 1.6% to 17.2% ± 6.0% in the moderate-binding regions and was unacceptably high for all methods in the low-binding regions.

Unlike the variability, the reliability, as determined by the ICC, was less dependent on the regional SERT density. The ICC for V_T was excellent (≈ 0.90) across all regions for the 1TC, 2TC, and DEPICT method. Similar values were observed for BP and V_3'', indicating these methods should work equally well at discriminating differences at the group level.

Determination of Model Order

The question of determination of model order is typically posed in terms of a tradeoff between better goodness of fit achieved with a higher-order model and better robustness to noise achieved with a lower-order model. With the present dataset, 1TC and 2TC yielded very similar outcome measure estimates across all subjects and regions. The statistics designed to test model order, the F ratio and the Akaike score, were fairly split between models. On the datasets that these statistics identified the 1TC fit as more parsimonious, it might be expected that the VAR statistic would be better for the 1TC model, but this was not the case (RM ANOVA, $P = 0.38$). Thus, we can recommend the 2TC over the 1TC, based on the observation that the 2TC fit is better for some datasets but there is no apparent loss of stability with 2TC compared with 1TC. In the context of this dataset, it was particularly interesting to examine the behavior of DEPICT. DEPICT is a method designed to estimate model order automatically and it was fairly split between 1TC and 2TC as well (a small number of fits were designated 3TC). The F ratio and Akaike score from the 1TC and 2TC models were not well correlated with DEPICT. For example, the mean F value from the regions designated 1TC by DEPICT was slightly but significantly higher than in those designated 2TC, with similar results for Akaike. The impulse response fraction is another parameter related to model order (37) that measures the fraction of the total area under the curve

resulting from the convolution of the input function with the faster of the 2 exponential functions in the response function of a 2TC model. It has been conjectured that very small impulse response fraction is associated with poor identifiability of 2 distinct compartments in a brain region. The impulse response fraction from the 2TC fits in the present dataset bear an intriguing relationship to model order as determined by DEPICT (Fig. 3). When the impulse response fraction is <0.01, the DEPICT model order is spread between 1TC and 2TC with all 4 3TC fits falling into this range as well. However, for 24 of the 29 fits for which the impulse response fraction is >0.005 and 13 of the 13 fits where the impulse response fraction is >0.01, the DEPICT model order estimate was 2. It remains for future work to further explore this relationship, particularly with ligands for which the impulse response fraction is more heterogeneous.

Evaluation of Graphical Analysis

Distribution volumes derived by graphical analysis were strongly correlated with V_T derived by both the 1TC and 2TC models ($r^2 = 0.99$, $P = 0.0001$, $n = 180$), with similar values of V_T (99.2% ± 2.5%), excellent test/retest variability (< 10%) and ICC (≈ 0.90). Unlike Ginovart et al., we did not find study-wide reduction in the values of V_T derived with the graphical analysis when compared with the kinetic analysis (2). We have reported a tendency for this method to underestimate V_T values in the past (38), but this
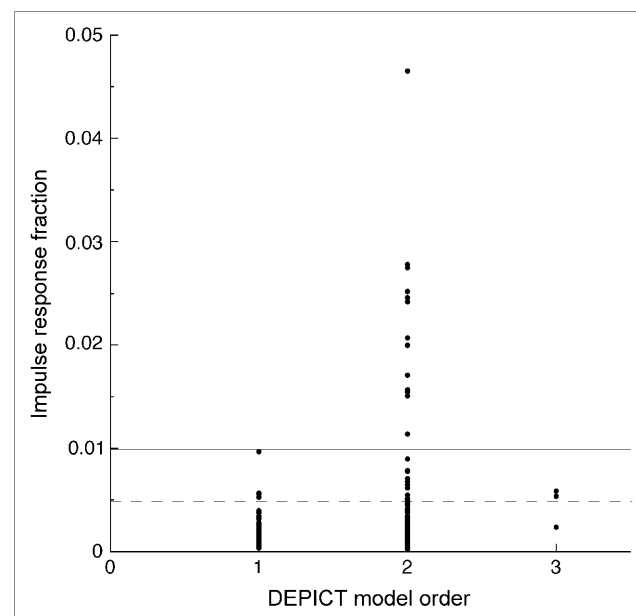
FIGURE 3. Relationship between impulse response fraction (IRF) generated from kinetic 2TC data and model order chosen by DEPICT. In the case when the IRF is small (<0.005, below dashed horizontal line), model order is spread between 1TC and 2TC without clear bias toward one or the other. However, for IRF of >0.005, the DEPICT method settled nearly exclusively on the 2TC model. This is particularly evident for IRF of >0.01 (above solid horizontal line).

is a statistical property, rather than a systematic property, of the method and was not evident in the present dataset. As with the kinetic analyses, the variability for the outcome measures BP and V_3'' with the graphical analysis was similar to V_T in the high-binding regions (10.6% $\pm$ 4.3%) and lower in the limbic (18.4% $\pm$ 7.1%) and neocortical (41.7% $\pm$ 11.1%) regions. The ICC of both BP and V_3'' for the graphical analysis was good across all regions (> 0.75).

Evaluation of SRTM

SRTM provided values of V_3'' that, in most regions, were similar to those achieved with the 1TC and 2TC models. However in MID, both the iterative and basis function approach produced lower estimates by 10%$-$15% compared with the 1TC and 2TC, as observed in a previous study (2). In addition, the reliability of the iterative implementation was noticeably lower than other methods, including basis function SRTM, particularly in the moderate and low-binding regions. Also, though no method had acceptable reliability in the low-binding regions, the iterative SRTM produced V_3'' estimates in low-binding regions that were clearly out of line with all other methods in select cases, although the average values remained similar, and was associated with unacceptably poor identifiability in these regions. It is not unexpected for basis function implementations to be more robust in high-noise situations (39), but the present study lends emphasis to the observation that basis function implementations are more stable when low signal-to-noise ratio derives not just from random error but from situations where specific binding comprises a small fraction of the signal.

CONCLUSION

The results of this study indicate that ^{11}C-DASB can be used to measure SERT parameters with high reproducibility in receptor-rich, central regions of the brain, with somewhat less, yet still acceptable, reproducibility in regions of moderate SERT density and poor reproducibility in low-density regions. No clear advantage was evident in the choice of analytic methods, as all methods examined gave similar values across all regions. Therefore, the choice of methods is dependent on the experimental situation, with some caveats. Examination of the 1TC and 2TC fits indicates that the higher-order model may provide a better fit in some studies. Alternatively, the DEPICT method offers a convolution algorithm approach that makes no a priori assumptions regarding model order, albeit with a small amount of bias in the highest binding regions induced by the truncation of the basis set away from the slowest washout rates. In the absence of an arterial input function, SRTM provides an alternative method of analysis, subject to the limitations imposed by the possibility of different levels of nonspecific binding across populations (40). Finally, the basis function implementation of SRTM pro-vides better reliability than the iterative version of this method, particularly in low- and moderate-binding regions, subject again to a small amount of bias in the highest binding regions.

REFERENCES

1. Wilson AA, Ginovart N, Schmidt M, Meyer JH, Threlkeld PG, Houle S. Novel radiotracers for imaging the serotonin transporter by positron emission tomography: synthesis, radiosynthesis, and in vitro and ex vivo evaluation of ^{11}C-labeled 2-(phenylthio)araalkylamines. *J Med Chem.* 2000;43:3103–3110.
2. Ginovart N, Wilson AA, Meyer JH, Hussey D, Houle S. Positron emission tomography quantification of [^{11}C]-DASB binding to the human serotonin transporter: modeling strategies. *J Cereb Blood Flow Metab.* 2001;21:1342–1353.
3. McCann UD, Szabo Z, Seckin E, et al. Quantitative PET studies of the serotonin transporter in MDMA users and controls using [^{11}C]McN5652 and [^{11}C]DASB. *Neuropsychopharmacology.* 2005;30:1741–1750.
4. Meyer JH, Houle S, Sagrati S, et al. Brain serotonin transporter binding potential measured with carbon 11-labeled DASB positron emission tomography: effects of major depressive episodes and severity of dysfunctional attitudes. *Arch Gen Psychiatry.* 2004;61:1271–1279.
5. Frankle WG, Narendran R, Huang Y, et al. Serotonin transporter availability in patients with schizophrenia: a positron emission tomography imaging study with [^{11}C]DASB. *Biol Psychiatry.* 2005;57:1510–1516.
6. Lammertsma AA, Hume SP. Simplified reference tissue model for PET receptor studies. *Neuroimage.* 1996;4:153–158.
7. Gunn RN, Gunn SR, Turkheimer FE, Aston JA, Cunningham VJ. Positron emission tomography compartmental models: a basis pursuit strategy for kinetic modeling. *J Cereb Blood Flow Metab.* 2002;22:1425–1439.
8. Logan J, Fowler J, Volkow ND, et al. Graphical analysis of reversible radio-ligand binding from time-activity measurements applied to [N -^{11}C-methyl]-(-)-cocaine PET studies in human subjects. *J Cereb Blood Flow Metab.* 1990;10:740–747.
9. Frankle W, Huang Y, Hwang D-R, et al. Comparative evaluation of serotonin transporter radioligands [^{11}C]DASB and [^{11}C]McN 5652 in healthy humans. *J Nucl Med.* 2004;45:682–694.
10. Mawlawi OM, Weiss R, Shinn A, Pidcock J, Slifstien M, Laruelle M. Performance characteristics of a head immobilization device for PET imaging [abstract]. *J Nucl Med.* 1999;40(suppl):281P.
11. Abi-Dargham A, Simpson N, Kegeles L, et al. PET studies of binding competition between endogenous dopamine and the D1 radiotracer [^{11}C]NNC 756. *Synapse.* 1999;32:93–109.
12. Abi-Dargham A, Laruelle M, Seibyl J, et al. SPECT measurement of benzodiazepine receptors in human brain with [123-I]iomazenil: kinetic and equilibrium paradigms. *J Nucl Med.* 1994;35:228–238.
13. Gandelman MS, Baldwin RM, Zoghbi SS, Zea-Ponce Y, Innis RB. Evaluation of ultrafiltration for the free fraction determination of single photon emission computerized tomography (SPECT) radiotracers: β-CIT, IBF and iomazenil. *J Pharm Sci.* 1994;83:1014–1019.
14. Abi-Dargham A, Martinez D, Mawlawi O, et al. Measurement of striatal and extrastriatal dopamine D1 receptor binding potential with [^{11}C]NNC 112 in humans: validation and reproducibility. *J Cereb Blood Flow Metab.* 2000;20:225–243.

15. Woods RP, Cherry SR, Mazziotta JC. Rapid automated algorithm for aligning and reslicing PET images. *J Comput Assist Tomogr.* 1992;16:620–633.

16. Duvernoy H. *The Human Brain: Surface, Three-Dimensional Sectional Anatomy and MRI.* New York, NY: Springer-Verlag; 1991.

17. Talairach J, Tournoux P. *Co-Planar Stereotactic Atlas of the Human Brain: Three-Dimensional Proportional System—An Approach of Cerebral Imaging.* New York, NY: Theime Medical Publisher; 1988.

18. Killiany RJ, Moss MB, Nicholson T, Jolez F, Sandor T. An interactive procedure for extracting features of the brain from magnetic resonance images: the lobes. *Hum Brain Mapp.* 1997;5:355–363.

19. Kates WR, Abrams MT, Kaufmann WE, Breiter SN, Reiss AL. Reliability and validity of MRI measurement of the amygdala and hippocampus in children with fragile X syndrome. *Psychiatry Res.* 1997;75:31–48.

20. Pani L, Gessa GL, Carboni S, Portas CM, Rossetti ZL. Brain dialysis and dopamine: does the extracellular concentration of dopamine reflect synaptic release? *Eur J Pharmacol.* 1990;180:85–90.

21. Mawlawi O, Martinez D, Slifstein M, et al. Imaging human mesolimbic dopamine transmission with positron emission tomography. I. Accuracy and precision of D2 receptor parameter measurements in ventral striatum. *J Cereb Blood Flow Metab.* 2001;21:1034–1057.

22. Mintun MA, Raichle ME, Kilbourn MR, Wooten GF, Welch MJ. A quantitative model for the in vivo assessment of drug binding sites with positron emission tomography. *Ann Neurol.* 1984;15:217–227.

23. Slifstein M, Laruelle M. Models and methods for derivation of in vivo neuroreceptor parameters with PET and SPECT reversible radiotracers. *Nucl Med Biol.* 2001;28:595–608.

24. Levenberg K. A method for the solution of certain problems in least squares. *Q Appl Math.* 1944;2:164–168.

25. Chen S, Donoho D, Saunders M. Atomic decomposition by basis pursuit. *SIAM Review.* 2001;43:129–159.

26. Gunn RN, Lammertsma AA, Hume SP, Cunningham VJ. Parametric imaging of ligand-receptor binding in PET using a simplified reference region model. *Neuroimage.* 1997;6:279–287.

27. Cunningham VJ, Jones T. Spectral analysis of dynamic PET studies. *J Cereb Blood Flow Metab.* 1993;13:15–23.

28. Akaike H. A new look at the statistical model identification. *IEEE Trans Automat Contr.* 1974;AC19(6):716–723.

29. Landaw EM, DiStefano JJ 3rd. Multiexponential, multicompartmental, and noncompartmental modeling. II. Data analysis and statistical considerations. *Am J Physiol.* 1984;246:R665–R677.

30. Carson RE. Parameters estimation in positron emission tomography. In: Phelps ME, Mazziotta JC, Schelbert HR, eds. *Positron Emission Tomography: Principles and applications for the Brain and the Heart.* New York, NY: Raven Press; 1986:347–390.

31. Laruelle M, Vanisberg M, Maloteaux J. Regional and subcellular localization in human brain of [^{3}H]paroxetine binding, a marker of serotonin uptake sites. *Biol Psychiatry.* 1988;24:299–309.

32. Backstrom I, Bergstrom M, Marcusson J. High affinity [^{3}H]paroxetine binding to serotonin uptake sites in human brain tissue. *Brain Res.* 1989;486:261–268.

33. Cortes R, Soriano E, Pazos A, Probst A, Palacios JM. Autoradiography of antidepressant binding sites in the human brain: localization using [^{3}H]imipramine and [^{3}H]paroxetine. *Neuroscience.* 1988;27:473–496.

34. Laruelle M, van Dyck C, Abi-Dargham A, et al. Compartmental modeling of iodine-123-iodobenzofuran binding to dopamine D_2 receptors in healthy subjects. *J Nucl Med.* 1994;35:743–754.

35. Kirk RE. *Experimental Design: Procedures for the Behavioral Sciences.* Pacific Grove, CA: Brooks/Cole Publishing Co.; 1982.

36. Logan J, Fowler JS, Volkow ND, Wang GJ, Ding YS, Alexoff DL. Distribution volume ratios without blood sampling from graphical analysis of PET data. *J Cereb Blood Flow Metab.* 1996;16:834–840.

37. Carson RE, Kiesewetter DO, Jagoda E, Der MG, Herscovitch P, Eckelman WC. Muscarinic cholinergic receptor measurements with [^{18}F]FP-TZTP: control and competition studies. *J Cereb Blood Flow Metab.* 1998;18:1130–1142.

38. Slifstein M, Laruelle M. Effects of statistical noise on graphical analysis of PET neuroreceptor Studies. *J Nucl Med.* 2000;41:2083–2088.

39. Gunn RN, Sargent PA, Bench CJ, et al. Tracer kinetic modeling of the 5-HT1A receptor ligand [carbonyl-^{11}C]WAY-100635 for PET. *Neuroimage.* 1998;8:426–440.

40. Laruelle M, Slifstein M, Huang Y. Positron emission tomography: imaging and quantification of neurotransporter availability. *Methods.* 2002;27:287–299.

The Journal of NUCLEAR MEDICINE

Estimation of Serotonin Transporter Parameters with ^{11}C-DASB in Healthy Humans: Reproducibility and Comparison of Methods

W. Gordon Frankle, Mark Slifstein, Roger N. Gunn, Yiyun Huang, Dah-Ren Hwang, E. Ashlie Darr, Rajesh Narendran, Anissa Abi-Dargham and Marc Laruelle

This article and updated information are available at:
http://jnm.snmjournals.org/content/47/5/815

Information about reproducing figures, tables, or other portions of this article can be found online at:
http://jnm.snmjournals.org/site/misc/permission.xhtml

Information about subscriptions to JNM can be found at:
http://jnm.snmjournals.org/site/subscriptions/online.xhtml

SNMMI | SOCIETY OF NUCLEAR MEDICINE AND MOLECULAR IMAGING